Diamond grinding of cutting inserts: edge chipping, specific energy, wheel wear, and process optimization

Citation for the original published paper (version of record):
Ventura, C., da Silva, E., Drazumeric, R. et al (2026). Diamond grinding of cutting inserts: edge chipping, specific energy, wheel wear, and process
optimization. CIRP Journal of Manufacturing Science and Technology, 69: 191-199.
http://dx.doi.org/10.1016/j.cirpj.2026.06.002

CIRP Journal of Manufacturing Science and Technology 69 (2026) 191–199

Contents lists available at ScienceDirect

CIRP Journal of Manufacturing Science and Technology

journal homepage: www.elsevier.com/locate/cirpj

Diamond grinding of cutting inserts: edge chipping, specific energy, wheel wear, and process optimization

Carlos E.H. Ventura [a], Eraldo Janone da Silva [b], Radovan Dražumerič [c], Jeffrey Badger [d], Peter Krajnik [e,*]

[a] Federal University of São Carlos, Department of Mechanical Engineering, Rod. Washington Luis km 235, São Carlos, SP 13565-905, Brazil
[b] University of São Paulo, São Carlos School of Engineering, Av. Trabalhador São-Carlense 400, São Carlos, SP 13566-590, Brazil
[c] University of Ljubljana, Faculty of Mechanical Engineering, Aškerčeva cesta 6, Ljubljana 1000, Slovenia
[d] The Grinding Doc, San Antonio, TX, USA
[e] Chalmers University of Technology, Department of Mechanical Engineering, Hörsalsvägen 7B, Gothenburg 412 96, Sweden

ARTICLE INFO

Keywords:
Grinding
Cutting tool
Insert
Geometry
Kinematic
Model
Optimization
Control
Energy efficiency
Wear

ABSTRACT

Diamond grinding of cutting-inserts was modeled and optimized by taking into account the varying position-dependent contact conditions along the nose radius. The results demonstrate that the dimensionless aggressiveness number correlates strongly with specific grinding energy and G-ratio while edge chipping along the nose radius shows no systematic dependence on process geometry and kinematics. A constant-aggressiveness grinding strategy, implemented by varying the insert angular speed, significantly reduces the total grinding energy and reduces the cycle time with no deterioration of edge quality. Overall, the developed physical models provide a robust, wheel-topography-independent framework for analyzing and optimizing grinding of cutting inserts.

1. Introduction

Cemented tungsten carbide (WC-Co) is the dominant substrate material for cutting inserts and is typically machined to its final geometry by diamond grinding, alongside other tool materials such as ceramics, polycrystalline cubic boron nitride (PCBN), and polycrystalline diamond (PCD). Since the performance of cutting tools is strongly governed by the resulting surface integrity, considerable effort has been devoted to improving grinding methods so that cutting-tool materials can be machined efficiently while maintaining acceptable surface finish and subsurface properties.

Research on diamond grinding of cutting-tool materials has largely concentrated on WC-Co. In industrial practice, however, cemented carbides, ceramics, PCBN, and PCD indexable inserts are typically ground on the same types of CNC insert grinders, using similar grinding kinematics and dressing strategies. Within this context, two complementary lines of research can be distinguished. One focuses on grindability and grinding mechanisms, i.e., how the grinding process affects workpiece surface integrity and the associated abrasive-workpiece interactions (e.g., plastic flow, crack propagation). The other advances fundamental process understanding through modeling, with emphasis on specific grinding energy and the role of grinding-wheel topography.

Hegeman et al. [1] and Ren et al. [2] reported that the material removal mechanism in WC-Co includes both brittle and ductile modes. In addition to crack formation, they observed fragmentation and pullout of carbide grains, as well as plastic deformation of the bonding material. According to Wirtz et al. [3], the Co content affects the grindability of WC-Co cemented carbides, with higher Co content leading to higher thermomechanical loads and wheel wear due to the increased adhesion, friction, and required energy associated with the more ductile nature of the binder material. Jiang et al. [4] investigated the effect of WC grain size and noted that its influence on workpiece quality was greater than that of different grinding parameters. Smaller WC grains resulted in reduced edge chipping and lower surface roughness.

During single-grit scratch tests, Klocke et al. [5] investigated the transition between brittle and ductile material removal in cemented carbides with different Co contents and observed that brittle removal predominated at higher chip thickness. Zhan and Xu [6] observed that the temperature rises exponentially as the chip thickness is reduced,

* Corresponding author.
E-mail address: peter.krajnik@chalmers.se (P. Krajnik).

https://doi.org/10.1016/j.cirpj.2026.06.002
Received 15 January 2026; Received in revised form 21 May 2026; Accepted 3 June 2026
Available online 10 June 2026

Nomenclature

*Aggr**	point-aggressiveness
Aggr'	line-aggressiveness
Aggr	aggressiveness-number
b	insert thickness
e	specific grinding energy
E	total grinding energy
F_t	tangential force
G-ratio	grinding ratio
h	local insert thickness
l_c	contact length
l_d	dressing path
Q	average material removal rate
Q'	specific material removal rate
r_ε	nominal nose radius
r_{local}	local nose radius
S_c	contact surface
Spk	reduced peak height
t_g	grinding time
v_{cd}	dressing cutting speed
v_{fa}	axial feed speed
v_{fad}	dressing axial feed speed
v_n	relative normal speed
v_R	insert tangential speed
v_s	grinding wheel cutting speed
v_t	relative tangential speed
x, y, z	coordinate system
α_o	insert clearance angle
a_x	radial infeed
Δr	edge chipping
ε	nose angle
φ	angular position along the nose radius
θ	opening angle
ω_R	insert angular speed

corroborating the results of Cruz et al. [7], who reported a decrease in compressive residual stresses with lower chip thickness.

Within this context, different approaches have been proposed to model the grinding process using undeformed chip thickness as a fundamental parameter. Agarwal and Rao [8] developed an analytical model based on the random distribution of the grit protrusion and real contact length, which considers the elastic deflections in the wheel-workpiece contact zone. The model was used to predict surface roughness, which is governed by the random geometry and the random distribution of cutting edges. By analyzing the grinding-wheel topography, Zhang et al. [9] proposed a model to describe the undeformed chip-thickness distribution considering grit distribution and grit protrusion. Using the model, they concluded that the surface roughness could be controlled by adjusting grit protrusion via dressing. Li et al. [10] developed an undeformed chip thickness model for vertical-spindle face grinding of tungsten and used it to simulate the ductile-brittle transition by accounting for the temperature dependence of the workpiece mechanical properties.

Reviewing precision grinding of axisymmetric aspherical optics, Yang et al. [11] identified the maximum undeformed chip thickness as a key parameter because of its great sensitivity to the ductile-brittle transition. In a study on the grinding of carbide inserts, Cai et al. [12] proposed a transient grinding-force model based on the grit element method. In this model, individual abrasive grits were discretized into elements, and forces were derived from wheel topography, grinding kinematics, cross-sectional cutting, wear-flat areas (including path interference), and the associated workpiece residual.

Despite the extensive work on modeling undeformed chip thickness at both the single-grit chip and process (macro) scale, direct experimental validation of the underlying equations remains difficult because individual grinding chips are hard to measure. Nevertheless, such models are widely used to analyze grinding performance. Their predictive capability is, however, limited because undeformed chip thickness depends not only on the process parameters, but also on the grinding-wheel topography. Key characteristics of the wheel topography, such as active cutting-point density, sharpness, and grit protrusion, are difficult to quantify. Also, they change continuously as the wheel wears, as shown by Macerol et al. [13] in their assessment of the effects of grit properties and dressing on grinding mechanics and wheel performance.

Therefore, from both a scientific and industrial perspective, there is a need for a robust descriptor that enables researchers and practicing engineers to quantify and control the grinding conditions along the cutting edge of inserts using only nominal geometry and kinematical parameters, without relying on detailed wheel-topography characterization.

Previous studies on the grinding of cutting inserts mainly considered plunge-face grinding and used the average single-grit chip thickness. To obtain values for different process conditions, Wobker [14] and Fritsch [15] neglected scratch superposition and grit wear and assumed a homogeneous geometry and protrusion height. To model the abrasive grits, Wobker considered a spherical geometry and treated as active only those grits with protrusion heights greater than half the grit size, whereas Fritsch applied a triangular geometry, with the number of active grits varying linearly with protrusion height. Friemuth [16] proposed a generic model and defined the abrasive geometry and protrusion height using the same assumptions and later extended this model to account for the contact length during grinding of the insert nose radius, enabling a more comprehensive determination of chip thickness.

Building on these works, Ventura et al. [17] showed that the trends in chip-thickness variation under different process conditions were similar, albeit with different values, regardless of the approach used to quantify grit geometry and cutting-point density. This confirmed that no single or universally “correct” value exists for chip thickness because it inherently depends on the grinding-wheel topography and the underlying assumptions. Therefore, this dependence complicates the use of chip-thickness-based models for process optimization in the grinding of cutting inserts.

To circumvent the necessity to measure or assume wheel-topography parameters (such as cutting-point density and the ratio of chip width to chip thickness), Badger [18] introduced a dimensionless aggressiveness number, *Aggr*. Subsequently, Dražumerič et al. [19] consolidated a theory of aggressiveness for arbitrary geometry and kinematics. Krajnik et al. [20] used *Aggr* to predict workpiece surface temperature in cam-lobe grinding and developed a constant-temperature strategy to minimize cycle time while avoiding thermal damage. In crankshaft grinding, Dražumerič et al. [21] established a relation between the specific grinding energy and *Aggr* and used it as a temperature-based method for selecting feed increments that prevent burn. Urgoiti et al. [22] also used the experimental relationship between specific energy and aggressiveness to estimate power and heat generated in face grinding with a straight wheel.

During insert grinding, inserts are typically rotated at constant angular speed. Because of this, the local radial infeed and contact length vary drastically along the nose radius. As a result, the grinding aggressiveness fluctuates around the cutting edge. These fluctuations give rise to local surges in material removal rate, increased wheel wear, and high energy consumption. To date, the varying contact geometry of peripheral grinding of indexable inserts has not been described using a position-dependent, dimensionless parameter along the nose radius. In the present work, the aggressiveness number is therefore employed as a fundamental parameter of grinding geometry and kinematics to quantify these local conditions without introducing wheel-topography parameters or attempting to predict grinding forces and surface roughness. This provides a robust, geometry-based framework for analyzing and optimizing diamond grinding of cutting inserts.

2. Analytical model of insert grinding

Four- and five-axis grinding machines equipped with diamond cup wheels are commonly used for peripheral grinding of indexable cutting inserts (Fig. 1) using the following sequence: (i) grinding of the straight faces; (ii) grinding of the nose radii (the blank rotates as the flat-face grinding wheel removes material); (iii) chamfer grinding (if necessary). The basic parameters are the cutting speed v_s (i and ii) and either axial feed v_{fa} (i) or insert angular speed ω_R (ii).

Analytical modeling is based on the theory of aggressiveness, introduced by Dražumerič et al. [19], adapted here to describe the contact geometry and corresponding kinematics between the grinding wheel and the workpiece, shown in Fig. 1. In the implemented theory, the fundamental parameter of abrasive interaction is the point-aggressiveness $Aggr^*$, defined as the ratio of the relative normal speed v_n to the relative tangential speed v_t, both acting relative to the grinding wheel.

$$Aggr^* = v_n/v_t \tag{1}$$

Following a given point on either the wheel or the workpiece as it traverses the abrasive contact, the concept is extended from a point to the corresponding contact line by defining (i) the specific material removal rate Q', and (ii) the line-aggressiveness $Aggr'$ as averages over the contact length l_c, according to Eqs. (2) and (3).

$$Q' = \frac{1}{l_c}\int_{l_c} v_n \mathrm{d}l_c \tag{2}$$

$$Aggr' = \frac{1}{l_c}\int_{l_c} Aggr^* \mathrm{d}l_c \tag{3}$$

Finally, the description is extended to the entire abrasive contact by calculating the material removal rate Q and the aggressiveness number $Aggr$ as averages over the contact surface (Eqs. (4) and (5)). The aggressiveness number is thus a fundamental geometric–kinematic parameter of the process and provides a basis for analyzing grinding outcomes such as specific energy and wheel wear.

$$Q = \frac{1}{S_c}\iint_{S_c} v_n \mathrm{d}S_c \tag{4}$$

$$Aggr = \frac{1}{S_c}\iint_{S_c} Aggr^* \mathrm{d}S_c \tag{5}$$

When grinding the straight faces of the insert, the aggressiveness-number $Aggr$ remains constant; it is simply the ratio of axial feed speed v_{fa} to grinding wheel cutting speed v_s. However, when grinding the insert nose radius, a more complex modeling is necessary because of instantaneous changes in the contact length around the nose radius.

For a cup grinding wheel (Fig. 2a), the abrasive layer is located on the nominally flat surface. Therefore, the local radius of curvature of the abrasive surface in the grinding plane is effectively infinite (Fig. 2b). The other parameters are: v_R = insert tangential speed, a_x = radial infeed, and α_o = insert clearance angle. For an arbitrary clearance angle, the nose radius depends on the variable h along the insert thickness ($0 \le h \le b$) (Fig. 2b). As a result, a conical surface is produced, and the nose

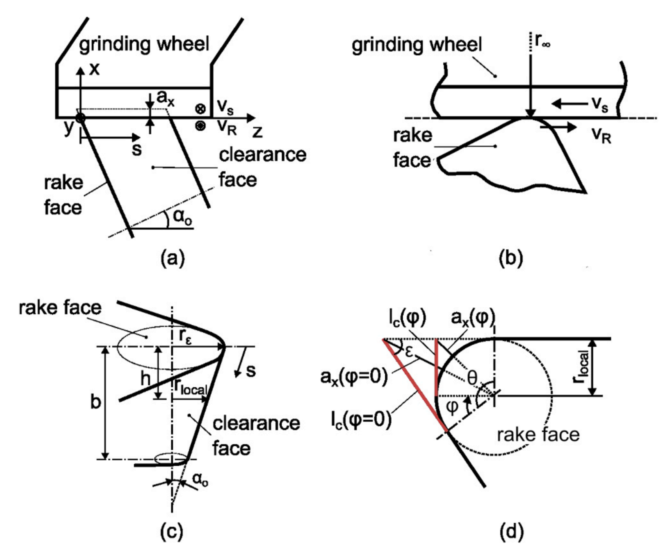

Fig. 2. (a) Top and (b) side views of the engagement area during grinding of the insert nose radius; (c) variation of the local nose radius r_{local} along the insert thickness; and (d) variation of the radial infeed a_x and the contact length l_c along the nose radius.

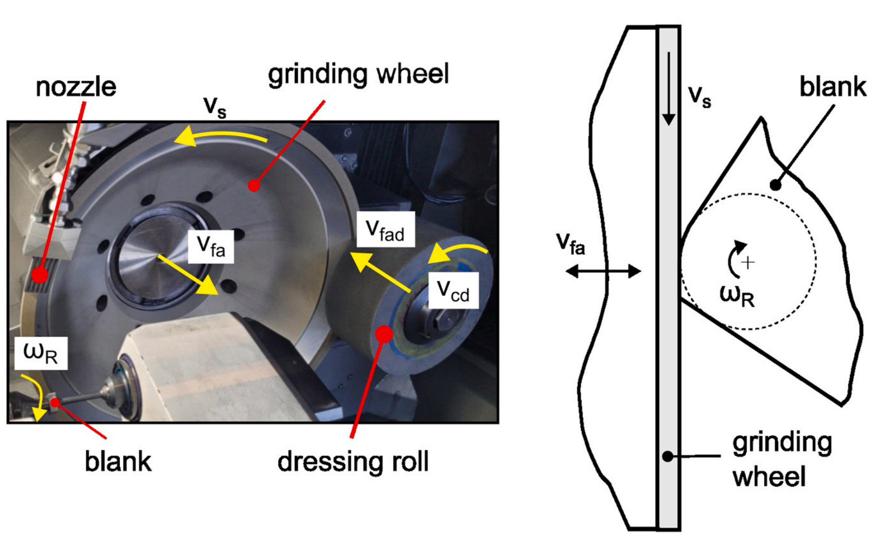

Fig. 1. Kinematics of insert grinding.

radius r_{local} (with r_ε = nominal nose radius) can be calculated by Eq. (6).

$$r_{local}(h) = r_\varepsilon - h\tan\alpha_0 \tag{6}$$

When grinding the insert nose radius, the tool-workpiece contact continuously changes along the nose radius due to insert rotation. The angular position φ along the radius varies from zero up to the opening angle θ ($0 \le \varphi \le \theta$) and can be related to the nose angle ε according to Eq. (7) and Fig. 2(d).

$$\theta = \pi - \varepsilon \tag{7}$$

Therefore, the radial infeed a_x and the corresponding contact length l_c assume different values along the s-axis and along the angular position φ. They can be calculated using Eqs. (8) and (9).

$$a_x(h,\varphi) = r_{local}(h)\left[1\Big/\sin\left(\frac{\varepsilon+\varphi}{2}\right) - 1\right] \tag{8}$$

$$l_c(h,\varphi) = \sqrt{2r_{local}(h)a_x(h,\varphi)/\cos\alpha_0} \tag{9}$$

The insert kinematics is given by the insert tangential speed v_R, which depends on the local nose radius $r_{local}(h)$ and the insert angular speed ω_R, according to Eq. (10).

$$v_R(h) = \omega_R r_{local}(h) \tag{10}$$

In conventional nose-radius grinding, ω_R is typically kept constant. Because the wheel-workpiece contact geometry varies with position along the nose radius, this leads to a position-dependent aggressiveness number.

Now, the normal component v_n and the tangential component v_t of speed acting relative to the grinding wheel can be determined by Eqs. (11) and (12).

$$v_n(y) = \omega_R y\cos\alpha_o \tag{11}$$

$$v_t(h) = |v_R(h) - v_s| \tag{12}$$

Based on the relative normal speed (Eq. (11)), and using the definitions in Eqs. (2) and (4) together with the contact-length expression in Eq. (9), the corresponding specific material removal rate and the material removal rate are given by Eqs. (13) and (14).

$$Q'(h,\varphi) = v_R(h)a_x(h,\varphi) \tag{13}$$

$$Q(\varphi) = Q'(b/2,\varphi)b/\cos\alpha_0 \tag{14}$$

The line-aggressiveness, *Aggr'*, which is the average point-aggressiveness of a given contact line at the position h, can be calculated by Eq. (15). Due to the particular process conditions, the line-aggressiveness is the same from the perspective of both the abrasive tool and the workpiece.

$$Aggr'(h,\varphi) = \frac{1}{|1 - v_s/v_R(h)|}\sqrt{\frac{a_x(h,\varphi)\cos\alpha_0}{2r_{local}(h)}} \tag{15}$$

For the optimization of the insert-nose grinding process, the aggressiveness number *Aggr* (Eq. (5)) must be determined. The aggressiveness number is the average point-aggressiveness of the contact surface and is approximated as $Aggr(\varphi) = Aggr'(b/2,\varphi)$. Finally, using Eqs. (6), (8), (10), and (15), and considering that $v_s >> v_R$, the final expression for the aggressiveness number is presented in Eq. (16).

$$Aggr(\varphi) = \frac{\omega_R(r_\varepsilon - b\tan\alpha_0/2)}{v_s}\sqrt{\left[1\Big/\sin\left(\frac{\varepsilon+\varphi}{2}\right) - 1\right]\frac{\cos\alpha_0}{2}} \tag{16}$$

The specific energy (Eq. (17)) was obtained by the measurement of the tangential force F_t and the application of Eq. (14).

$$e(\varphi) = \frac{F_t(\varphi)v_s}{Q(\varphi)} \tag{17}$$

3. Experimental work

Experiments were conducted on a four-axis insert grinding machine Agathon DOM Plus with a vitrified-bonded diamond cup wheel (grit size D46 and concentration C100) using a straight oil as grinding fluid. Before grinding each blank, the wheel was dressed with a 180-mesh alumina dressing roll (cutting speed $v_{cd} = 10$ m/s, axial feed speed $v_{fad} = 3$ μm/s, and dressing path $l_d = 15$ μm).

The workpiece material was cemented tungsten carbide, ISO grade K10 (with approximate dimensions 11.2 mm × 11.2 mm × 4.7 mm). The straight faces (clearance angle $\alpha_o = 0°$) were ground with a cutting speed $v_s = 35$ m/s and an axial feed speed $v_{fa} = 4$ mm/min. The nose radii (with a nose angle $\varepsilon = 90°$) were ground with the same cutting speed, radii $r_\varepsilon = 0.8$ mm and 1.2 mm, and angular speeds $\omega_R = 35°$/s and 60°/s.

The lower angular speed was selected based on industrial experience for grinding cemented carbide. The higher angular speed was chosen to increase the aggressiveness number and assess its influence on edge chipping; under this condition, the applied load is expected to be higher, while the grinding time is reduced.

The selected insert geometry (nose angle and nose radii) is representative of common designs. Larger nose radii increase the contact area and, consequently, the forces. At the same time, the selected geometry enables the acquisition of stable force signals during grinding over an adequate time window, allowing reliable data acquisition.

For negligible tool wear, as is the case when grinding each nose radius, previous studies have shown that edge quality and specific energy vary monotonically with changes in cutting and feed speeds [23]. In addition, the insert angular speed has been reported to have only a minor effect on edge quality across different nose regions [17], despite continuous changes in contact length and radial infeed. Therefore, only two parameter levels were selected to reflect these observations, with the primary objective of characterizing the variation of the output variables along the nose radius.

The first step was to determine the dependency on aggressiveness number of (a) edge chipping Δr, (b) specific grinding energy e, and (c) wheel wear (via *G-ratio*).

The edge chipping was measured using an optical, focus-variation microscope (Alicona InfiniteFocus SL). This quality parameter corresponds to the shortest distance between the real and ideal (perfectly sharp) cutting edge. The measurement consisted of 200 profiles distributed around the middle of the radius, covering a circular sector of 50°, as shown in Fig. 3. An average value was calculated (for four insert corners) for every ten measurements.

The tangential force was obtained using the machine's built-in monitoring system, which estimates the effective torque of the grinding spindle from the motor current and converts it to tangential force. Data was sampled at 50 Hz. Additional details were proprietary.

The grinding ratio G is the ratio of the volume of removed workpiece material to the volume of wheel wear. The workpiece volume was obtained from the difference between the initial and final workpiece dimensions. The wheel volume was obtained by direct measurement of the worn wheel profile (Fig. 4) at three different regions using the focus-variation microscope. In addition, the reduced peak height parameter, *Spk*, obtained from the material ratio (Abbott-Firestone) curve was measured in selected (1.5 ×2 mm^2) areas of the worn region to provide a local measure of grit protrusion. Here, the straight faces of the inserts were ground in a plunge-grinding operation.

4. Results and discussion

The variation of the aggressiveness number with angular position along the nose radius is shown in Fig. 5(a) and (b). In all cases, a continuous decrease in aggressiveness is observed, which can be explained by the evolution of the radial infeed a_x with higher values at the beginning of the process. As expected, an increase in the angular

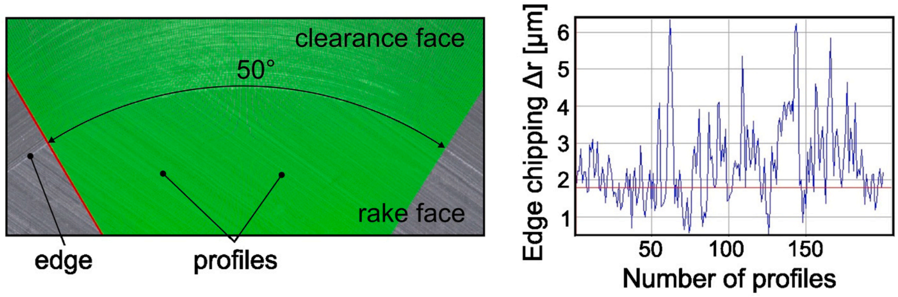

Fig. 3. Edge-chipping measurement.

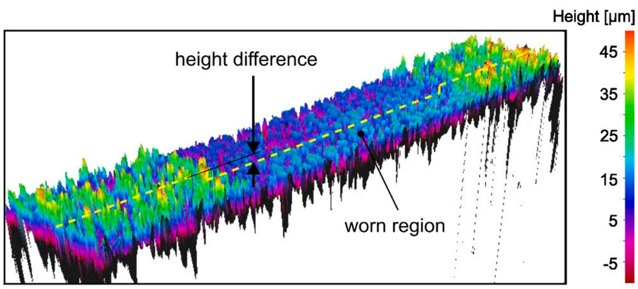

Fig. 4. Measurement of the worn wheel profile.

speed ω_R (Fig. 5a) and in the nose radius r_ε (Fig. 5b) shifts the curves upward and increases the aggressiveness, especially at smaller angular positions.

Edge-chipping results for the corresponding grinding conditions are presented in Figs. 5(c) and 5(d), taken around the middle region of the nose radius. Despite the relatively large range of aggressiveness values, no systematic trend of edge chipping can be identified; the measured values remain within a narrow band for all conditions. This is a significant experimental finding as it shows that edge chipping is largely independent of input parameters. For process design, this suggests that the edge-chipping constraint can be decoupled from the selection of aggressiveness aimed at productivity improvements.

Representative ground edges for the different nose radii are shown in Fig. 5(e), (f), and (g). Small, evenly distributed defects can be observed along the nose radius, which may reflect the high local scatter introduced by the changing wheel topography and the limited anchorage of WC hard particles in the Co binder [23]. Overall, the results indicate that edge chipping does not depend significantly on aggressiveness for the present wheel-workpiece combination and parameter range.

The relationship between specific grinding energy and aggressiveness number for grinding the nose radii is shown in Fig. 6. An exponential decrease in specific energy is observed, which is consistent with the size effect. At low aggressiveness values ($Aggr < 4 \times 10^{-6}$), measurements were erratic, and the specific energy became very high; this range is therefore denoted as an "unstable region". This figure also shows the two constant-aggressiveness conditions investigated in this work ($Aggr = 4.85 \times 10^{-6}$ and 12.0×10^{-6}), which lie in the stable region and avoid excessive diamond-workpiece rubbing and unnecessary cycle-time losses.

In addition to edge quality and specific energy, wheel wear is another key aspect to consider when evaluating process performance. The relationship between grinding-wheel-wear volume and volume of removed workpiece material for two aggressiveness conditions is shown in Fig. 7 (a). Increasing the aggressiveness number leads to a lower *G-ratio* due to the higher mechanical loading of the diamond grits and, possibly, increased binder wear. A fourfold increase in aggressiveness resulted in an approximately tenfold decrease in the *G-ratio*. The percentage deviation ranges from 9% to 12% at the higher aggressiveness level and from 12% to 16% at the lower level. In the latter case, the error bars are too small relative to the corresponding average values to be clearly visible in the plot.

The reduced peak height *Spk* measured in the worn regions, which provides a local measure of grit protrusion, decreased with increasing volume of removed material for both aggressiveness conditions (Fig. 7b), indicating progressive abrasive grit wear. Nevertheless, the 3D topographies of the worn wheel regions for the two aggressiveness levels (Figs. 7c and 7d) do not reveal a clear qualitative trend with removed volume, and no pronounced differences were observed between the abrasive layer before and after grinding with different material removal volumes. The grits retained a largely flattened appearance.

The findings indicate that edge chipping is not a critical constraint within the investigated range of grinding aggressiveness. However, the decrease in aggressiveness leads to higher values of specific energy, whereas increasing aggressiveness accelerates wheel wear and reduces *G-ratio*.

Effective process control should therefore aim at maintaining aggressiveness within an appropriate, approximately constant range. In nose-radius grinding, this is not straightforward because the local material removal rate and contact length change with angular position. Achieving a constant aggressiveness profile thus requires an adaptation of the process kinematics, which is examined in the following section.

5. Feasibility of process optimization using constant aggressiveness-number in the grinding of the insert nose radius

To optimize the process and avoid the "unstable region", it is necessary to select an appropriate aggressiveness number *Aggr*. To accomplish this, a strategy was developed to continuously vary the insert angular speed while keeping the wheel speed constant. The required angular speed to maintain a constant aggressiveness is given by Eq. (18), obtained from Eq. (16).

$$\omega_R(\varphi) = \frac{Aggr\; v_s}{(r_\varepsilon - b\tan\alpha_0/2)\sqrt{\left[1\Big/\sin\left(\frac{\varepsilon+\varphi}{2}\right) - 1\right]\frac{\cos\alpha_0}{2}}} \tag{18}$$

The grinding time t_g, which depends on the insert angular speed and the nose angle, can be calculated by Eq. (19):

$$t_g = \int_0^{\pi-\varepsilon} \frac{1}{\omega_R(\varphi)} \mathrm{d}\varphi \tag{19}$$

The total grinding energy E of insert-nose grinding is determined by Eq. (20), using Eqs. (8), (10), (13), (14), and (17).

$$E = \int_0^{\pi-\varepsilon} \frac{F_t(\varphi)v_s}{\omega_R(\varphi)} \mathrm{d}\varphi = r_{local}^2 (b/2) b \int_0^{\pi-\varepsilon} e(\varphi)\left[1\Big/\sin\left(\frac{\varepsilon+\varphi}{2}\right) - 1\right] \mathrm{d}\varphi \tag{20}$$

For a given insert geometry, this expression shows that the total energy depends only on the specific grinding energy. Grinding at constant aggressiveness avoids the unstable region of high specific energy and is therefore more energy efficient.

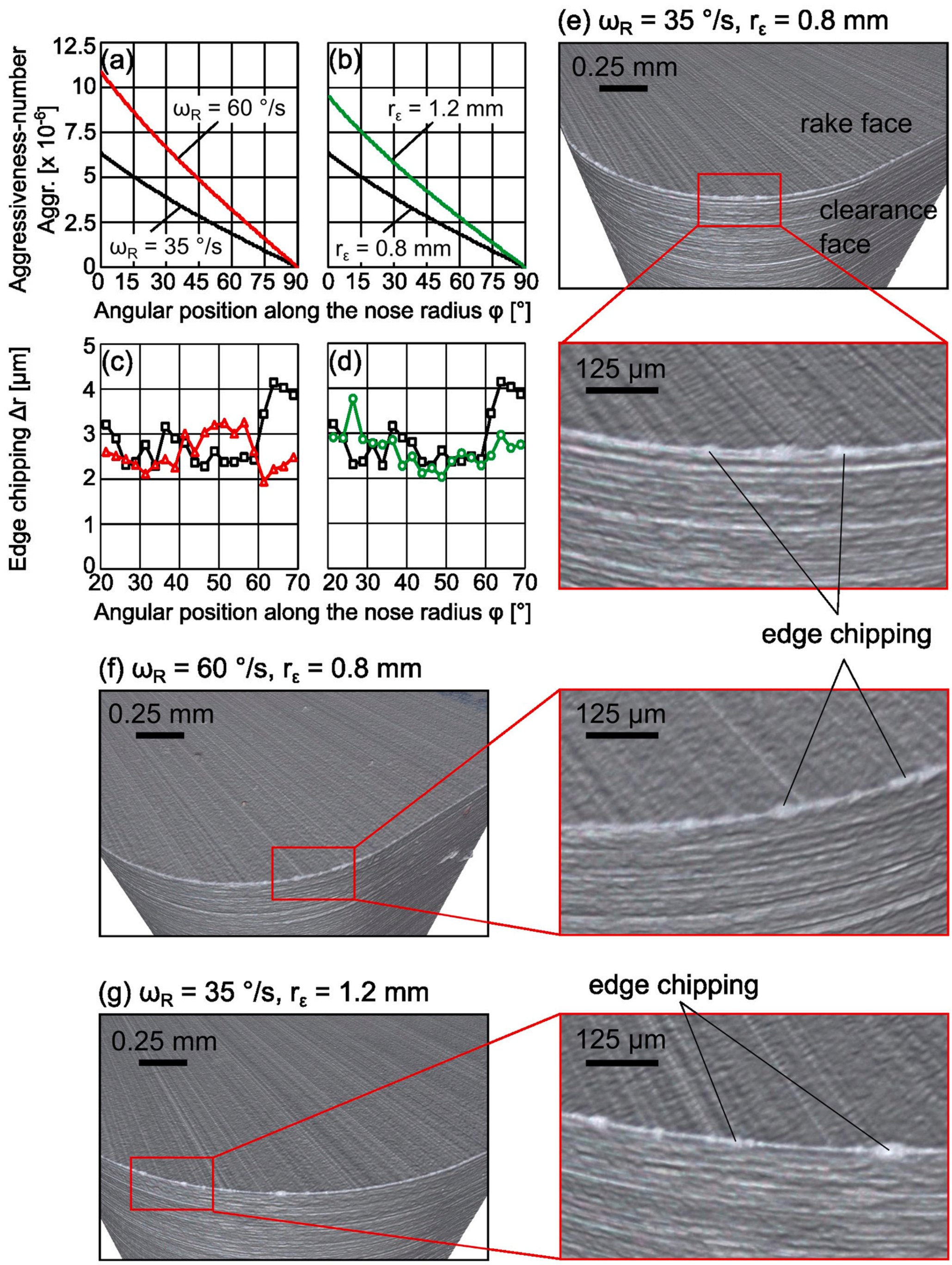

Fig. 5. Variation of the aggressiveness-number *Aggr* and edge chipping Δr along the nose radius with a variation of (a, c) insert angular speed ω_R ($r_\varepsilon = 0.8$ mm) and (b, d) nose radius r_ε ($\omega_R = 35$ °/s); (e, f, g) 3D images of the edges along the nose radius with different insert angular speeds and nose radii.

Considering the conditions $\alpha_o = 0°$, $\varepsilon = 90°$, $r_\varepsilon = 1.2$ mm, $v_s = 35$ m/s, and $Aggr = 4.85 \times 10^{-6}$ (at the transition region of the specific energy curve), and $Aggr = 12 \times 10^{-6}$ (corresponding to a much lower specific energy, see Fig. 6), the continuous lines in Fig. 8(a) are obtained, representing the insert angular speed for the two constant-aggressiveness values.

As aggressiveness approaches zero near the end of nose-radius grinding (see Fig. 5a and b), the angular speed needed to achieve a constant aggressiveness becomes very high. This cannot be realized in practice due to the machine's maximum angular speed limitation (200°/s). Moreover, a truly continuous variation of angular speed is not feasible because of CNC programming constraints. Therefore, to approximate a constant aggressiveness along most of the nose radius, the curves presented in Fig. 8(a) (continuous lines) were discretized into angular-speed levels (line + symbol) within the range of $0 < \omega_R < 200°$/s. Neglecting the time required for acceleration between levels, the resulting stepwise angular speed and corresponding grinding time evolution are shown in Fig. 8(a) and (b). Curves for a constant angular speed ($\omega_R = 60°$/s, dotted green line) are included for comparison.

The total grinding energy consumed in tests with constant and variable angular speeds (constant aggressiveness) was determined by integrating the product of the tangential force and cutting speed over the grinding time. The calculated values (Fig. 9) show that the proposed strategy drastically reduces energy consumption (by approximately 84%). This is accompanied by a longer grinding time for the lower aggressiveness level (increase of ~43%) and a shorter cycle time for the

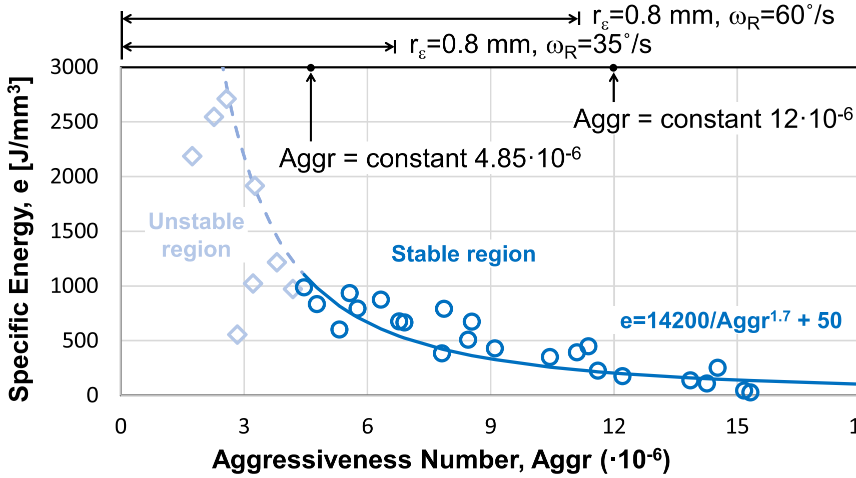

Fig. 6. Specific energy *e* vs. aggressiveness-number *Aggr*.

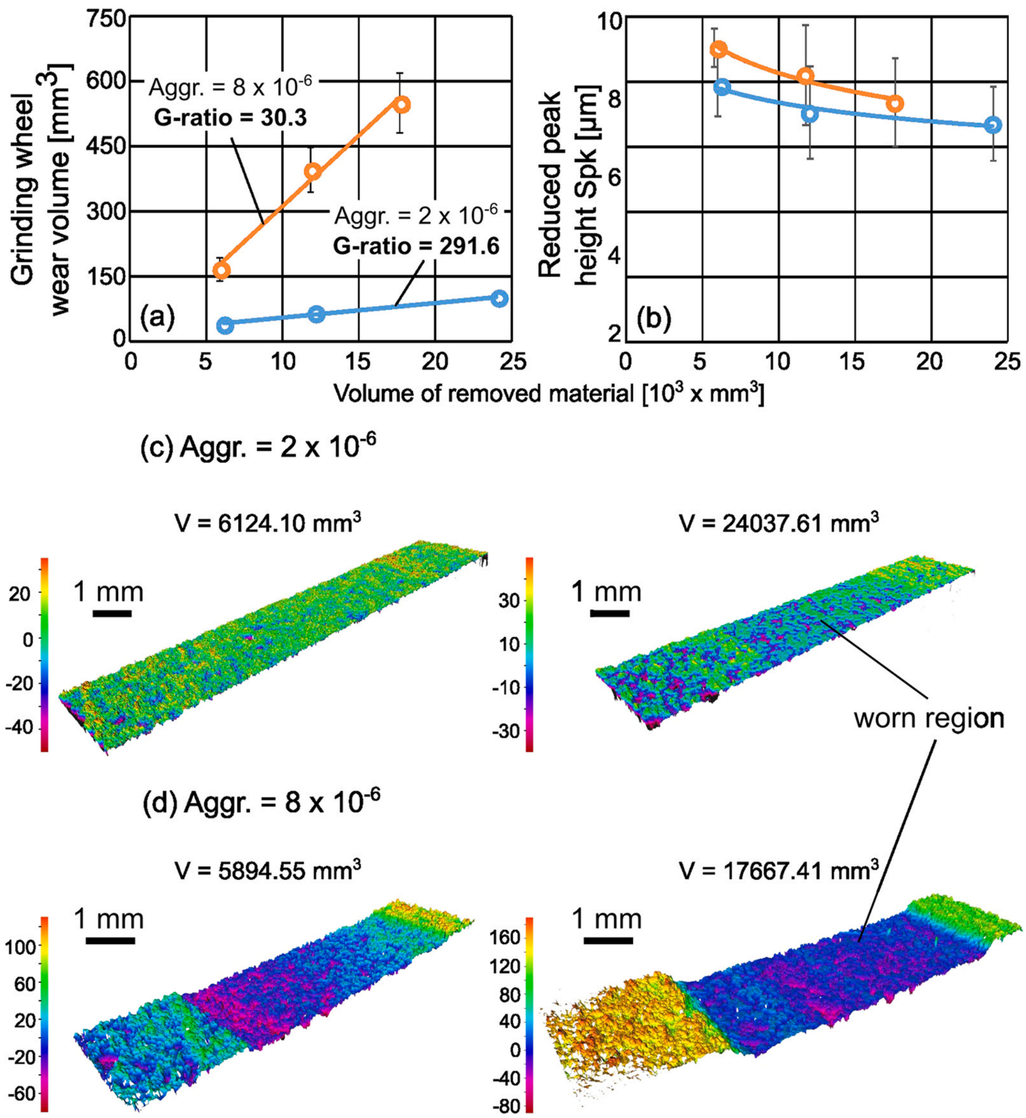

Fig. 7. Obtained (a) *G-ratios*, (b) reduced peak heights *Spk* for different aggressiveness-numbers *Aggr*, and (c, d) grinding wheel topographies after different material removal volumes.

higher aggressiveness level (decrease of ~37%). Owing to limitations related to machine dynamics, the low acquisition rate of the force signal,

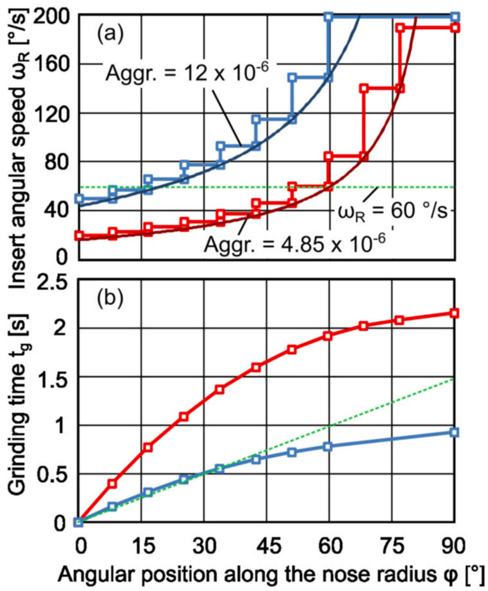

Fig. 8. (a) Theoretical (continuous line) and programmed (line + symbol) insert angular speed ω_R along the nose radius for two constant aggressiveness values $Aggr = 4.85 \times 10^{-6}$ and $Aggr = 12 \times 10^{-6}$, and (b) corresponding grinding time t_g.

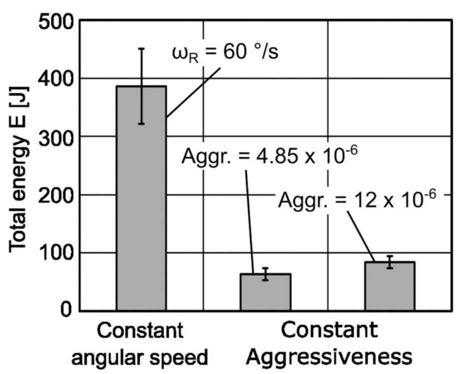

Fig. 9. Total grinding energy E consumed in grinding of the insert nose radius with constant aggressiveness $Aggr$ and angular speed ω_R.

and the combination of higher angular speeds with shorter contact lengths, it was not possible to reliably resolve the tangential-force variations (and therefore specific energy) associated with different angular-speed segments.

6. Conclusions

Based on the modeling and experiments, the following conclusions are drawn:

- The developed models demonstrate that the aggressiveness number provides a robust framework for quantifying insert grinding; it is capable of accounting for variations in contact geometry and kinematics.
- Modeling allows the identification of (i) low-aggressiveness regions along the nose radius, where feed rates can be increased, and (ii) high-aggressiveness regions, where feed rates can be reduced, leading to an overall reduction of cycle time and wheel wear.
- Within the tested range, edge chipping varied only within a narrow band and showed no systematic dependence on aggressiveness or angular position. This suggests that edge-chipping constraints can be excluded from aggressiveness-based optimization.
- The specific energy along the nose radius exhibits an exponential relationship with changes in the aggressiveness number.
- An increase in the aggressiveness number was associated with a decrease in the *G-ratio*, showing that higher aggressiveness improves energy efficiency but accelerates wheel wear, while edge quality remains essentially unchanged. This quantifies a key trade-off for selecting the operating window in industrial insert grinding.
- A discretized angular-speed profile was implemented to approximate constant aggressiveness along most of the nose radius within machine limitations. Experiments confirmed that this strategy can reduce the total grinding energy by about 84%, with only moderate changes in cycle time (longer at low aggressiveness, shorter at high aggressiveness) and no deterioration in edge chipping.
- Overall, the results demonstrate that the developed modeling framework is capable of analyzing and optimizing insert grinding – linking process geometry and kinematics to energy requirements and wheel wear. Because it relies only on nominal process parameters, the approach is directly transferable to other superhard insert materials (e.g., PCBN, PCD) without the need for a detailed wheel-topography characterization.

These above results also indicate the following practical implications and directions for further work.

Small anchorage of carbide grains at the edge reduces the sensitivity of edge quality to process parameters. Therefore, reduced edge chipping should be obtained primarily by improvements in tool material properties (e.g., increased fracture toughness) rather than by process optimization.

Maintaining constant aggressiveness along the entire nose radius is limited by the machine's maximum angular speed. However, the lack of fully continuous angular-speed profile (discretization) was not an issue because changes in angular speed during insert rotation could be neglected due to the very high acceleration/deceleration provided by the machine.

Future work should address the application of the theory of aggressiveness to plunge-face dressing processes typically employed in insert grinding machines. This would allow the determination of the influence of a combined aggressiveness number (for dressing and grinding) on grinding outputs without the need for wheel-topography characterization.

CRediT authorship contribution statement

Drazumeric Radovan: Writing – review & editing, Methodology, Formal analysis. **Jeffrey Badger:** Writing – review & editing, Visualization, Conceptualization. **Peter Krajnik:** Writing – review & editing, Supervision, Resources, Project administration, Conceptualization. **Ventura Carlos Eiji Hirata:** Writing – original draft, Visualization, Resources, Methodology, Investigation, Funding acquisition, Formal analysis. **Eraldo Janone da Silva:** Writing – review & editing, Investigation, Funding acquisition.

Declaration of Competing Interest

The authors declare that they have no known competing financial interests or personal relationships that could have appeared to influence the work reported in this paper.

Acknowledgements

Financial support from the Brazilian National Council for Scientific and Technological Development (CNPq, grant numbers 305730/2022–3 and 308566/2021–1), the São Paulo Research Foundation (FAPESP, grant numbers 2024/04833–1, 2017/12309–7, and 2017/12304–5), and the Slovenian Research and Innovation Agency (Research program P2–0266) is gratefully acknowledged. The authors also thank Sandvik Coromant for valuable technical discussions and industrial insights.

References

[1] Hegeman JBJW, De Hosson JTM, With G. Grinding of WC-Co hardmetals. Wear 2001;248:187–96.
[2] Ren YH, Zhang B, Zhou ZX. Specific energy in grinding of tungsten carbides of various grain sizes. CIRP Ann Manuf Technol 2009;58:299–302.
[3] Wirtz C, Dehmer A, Trauth D, Mattfeld P, Klocke F. Analysis of the grinding wheel wear in dependency of the cemented carbide specification. Int J Adv Manuf Technol 2018;99:747–54.
[4] Jiang Y, Zhou M, Zhan L, Tian Y, Yang M, Zhu Y, et al. Research on cutting tools edge grinding damage of nano cemented carbide. Wear 2025;578 – 579:206213.
[5] Klocke F, Wirtz C, Mueller S, Mattfeld P. Analysis of the material behavior of cemented carbides (WC-Co) in grinding by single grain cutting tests. Proc Cirp 2016;46:209–13.
[6] Zhan YJ, Xu XP. An experimental investigation of temperatures and energy partition in grinding of cemented carbide with a brazed diamond wheel. Int J Adv Manuf Technol 2012;61:117–25.
[7] Cruz DC, Christoforo AL, Sordi VL, Ventura CEH. Inducement of residual stresses in WC-5%Co cutting inserts by plunge-face grinding. Int J Adv Manuf Technol 2021;113:553–63.
[8] Agarwal S, Rao PV. Predictive modeling of undeformed chip thickness in ceramic grinding. Int J Mach Tools Manuf 2012;56:59–68.
[9] Zhang Y, Fang C, Huang G, Xu X. Modeling and simulation of the distribution of undeformed chip thicknesses in surface grinding. Int J Mach Tools Manuf 2018;127:14–27.
[10] Li G, Kang R, Wang H, Bao Y, Wang Y. Undeformed chip thickness models for precise vertical-spindle face grinding of tungsten heavy alloy. Prec Eng 2024;88:970–85.
[11] Yang W, Chen B, Guo B, Zhao Q, Dai J, Qing G. Research progress on grinding contact theory of axisymmetric aspheric optical elements. Prec Eng 2026;97:24–51.
[12] Cai S, Yao B, Zheng Q, Cai Z, Feng W, Chen B, et al. Dynamic force model for carbide insert peripheral grinding based on grain element method. J Manuf Process 2020;58:1200–10.
[13] Macerol N, Franca LFP, Drazumeric R, Krajnik P. The effects of grit properties and dressing on grinding mechanics and wheel performance: Analytical assessment framework. Int J Mach Tools Manuf 2022;180:103919.
[14] H.-G. Wobker, Schleifen keramischer Schneidstoffe, Ph.D. Thesis. Hannover University, 1992. (in German).
[15] A. Fritsch, Schleifen von Cermets, Ph.D. Thesis. Hannover University, 1997. (in German).
[16] T. Friemuth, Schleifen hartstoffverstärkter keramischer Werkzeuge, Ph.D. Thesis. Hannover University, 1999. (in German).
[17] Ventura CEH, Köhler J, Denkena B. Strategies for grinding of chamfers in cutting inserts. Prec Eng 2014;38:749–58.
[18] Badger J. Practical application of aggressiveness and chip thickness in grinding. CIRP 3rd International Conference on High Performance Cutting (HPC), Dublin, Ireland. 2008. p. 599–606.
[19] Drazumeric R, Badger J, Roininen R, Krajnik P. On geometry and kinematics of abrasive processes: The theory of aggressiveness. Int J Mach Tools Manuf 2020;154:1–13.
[20] Krajnik P, Drazumeric R, Badger J, Hashimoto F. Cycle optimization in cam-lobe grinding for high productivity. CIRP Ann 2014;63:333–6.
[21] Drazumeric R, Roininen R, Badger J, Krajnik P. Temperature-based method for determination of feed increments in crankshaft grinding. J Mater Process Technol 2018;259:228–34.
[22] Urgoiti L, Barrenetxea D, Antonio-Sánchez J, Lanzagorta JL. Detailed thermo-kinematic analysis of face grinding operations with straight wheels. Met 2020;10:1–13.
[23] Cruz DC, Sordi VL, Ventura CEH. Surface analysis of WC-5%Co cemented tungsten carbide cutting insert after plunge-face grinding. Int J Adv Manuf Technol 2020;108:323–30.